Transient Mechanical Test Development for Accident Tolerant Cladding Candidates to Simulate PCMI-like Conditions[1]

M. Nedim Cinbiz[1], Kurt A. Terrani[1], Nicholas Brown[1,2] and Kory Linton[1]
[1]Oak Ridge National Laboratory P.O. Box 2008, Oak Ridge, TN 37831-6156, USA
[2] The Pennsylvania State University, 229 Reber Building, University Park, PA 16802, USA

ABSTRACT*:* This study investigates the transient mechanical response of accident tolerant fuel cladding candidates to provide information on potential pellet-clad mechanical interaction induced deformation and failure of candidate cladding materials. The mechanical testing is applied to Gen-I FeCrAl and triaxially-braided SiC fiber SiC matrix composite materials under loading conditions like the pellet-clad mechanical interaction during a postulated design basis reactivity insertion accident. To achieve the specific loading conditions, a modified burst test instrument with accurate mechanical pulse control has been designed and constructed. The mechanical responses of FeCrAl, SiC-SiC composite tubes were compared with the pre-hydrided zirconium alloy cladding. The specimens subjected to mechanical pulses were investigated in a strain-controlled manner deformation.

KEYWORDS*: Accident-tolerant fuel, SiC/SiC composites, FeCrAl alloys, reactivity initiated accident, rapid loading, pellet-clad interaction, modified burst test*

I. INTRODUCTION[2]

The beyond-design-basis accident (BDBA) at the Fukushima Daiichi nuclear power plant after Tohoku earthquake and aftermath tsunami boosted the advance accident-tolerant fuel **(ATF)** technologies to replace current nuclear fuel materials and core components in service. Several materials are being considered as ATF cladding to zirconium-based alloy cladding. This includes silicon carbide fiber silicon carbide matrix composite structures (SiC/SiC) and iron-chromium-aluminum (FeCrAl) alloys [1,2]. Candidate ATF materials must enhance performance during beyond design basis accidents by increasing the amount of coping time without active cooling during the severe accident. For ATF cladding candidates, this is typically accomplished by improving high-temperature steam oxidation resistance [3]. In addition to the enhanced BDBA tolerance, candidate ATF materials must preserve the present safety characteristics during postulated design-basis accidents such as loss-of-coolant and reactivity-initiated accident (RIA) [4]. Due to their high mechanical strength at elevated temperatures under in the range of 800°C to 1000°C steam environment, ATF cladding candidates such as FeCrAl alloys and SiC/SiC are anticipated to extend the cladding burst margins during a loss-of-coolant accident (LOCA) [5]. However, the mechanical response of these alloys has not been yet tested under conditions that emulate those caused by an RIA.

---

[1] Notice: This manuscript has been authored by UT-Battelle, LLC under Contract No. DE-AC05-00OR22725 with the U.S. Department of Energy. The United States Government retains and the publisher, by accepting the article for publication, acknowledges that the United States Government retains a non-exclusive, paid-up, irrevocable, world-wide license to publish or reproduce the published form of this manuscript, or allow others to do so, for United States Government purposes. The Department of Energy will provide public access to these results of federally sponsored research in accordance with the DOE Public Access Plan (http://energy.gov/downloads/doe-public-access-plan).

[2] Some material in the manuscript was published in a conference proceedings [22] and a recent journal article [23]. The FeCAl and ZIRLO experiments has been published in [22,23]. The design of the instrument that is capable of to control the mechanical pulse shape has been published in [23] This manuscript extends the experimental study to SiC/SiC composites including the results obtained from other ATF cladding candidates and discusses the results in a manner of failure modes of different ATF candidate samples.

During an RIA, positive reactivity can be inserted as result of control rod removal from the reactor core. Because of the positive reactivity, the fission rate exponentially increases until the power pulse is turned around by fuel temperature feedback due to the Doppler broadening effect.

The thermal energy deposition during RIA causes a rapid temperature increase in fuel pellets, which results in thermal expansion of the fuel. If the fuel-cladding gap has closed or closes during the event, the expansion of the fuel cause pellet-clad mechanical interaction (PCMI) and thus impose a strain on the cladding. The power pulse occurs on a time scale of tens of milliseconds and may cause cladding failure if the cladding is sufficiently strained. The General Design Criteria require maintaining the integrity of the coolant pressure boundary and the core-cooling capability [6]. Thus, the mechanical response of ATF cladding must be investigated under RIA-induced PCMI deformation.

This study investigates the PCMI during postulated RIA or RIA-like transients by conducting separate effects tests on selected ATF cladding candidates and a zirconium-based cladding (ZIRLO^{TM}) alloy for comparison. To perform mechanical testing for the PCMI phase of RIA-like transients, a mechanical test instrument is built that is capable of finely tune the mechanical pulse shape. The device is based on an improved version of a modified-burst test device design developed by Yueh et al. [7]. Selected ATF cladding materials (Gen-I FeCrAl and SiC/SiC composite) and ZIRLO^{TM} cladding were subjected to the same mechanical loading. Evolution of hoop strain on the sample surface were in situ monitored by strain gauge attached to the sample. The failure mode and fracture behavior of the samples were discussed in terms of the changes in the hoop strain and the damage accumulation.

II. MATERIALS

This study utilizes two types of candidate ATF cladding materials (Gen-I FeCrAl and SiC/SiC composite) and ZIRLO cladding as shown in Fig. 1. FeCrAl (Fe-11.9Cr-5.98Al-0.02Y) samples with grain size of 100 μm had an outer diameter of 8.63 mm and a wall thickness of 0.44 mm. FeCrAl samples were without no solid solution strengthening or precipitation hardening (see [8] for alloy details).

SiC/SiC composite samples General Atomics' triaxially-braided SiC/SiC architecture of Hi Nicalon^{TM} type S fibers with pyrolithic carbon (PyC) interphase for cladding tube applications. PyC was initially deposited via chemical vapor deposition (CVD) on the preform SiC fibers. Fibers bundles were oriented 0° and ±45° with the tube axial direction as shown in Fig. 1. The SiC/SiC was fabricated by chemical vapor infiltration (CVI). The initial porosity of fibers is 10%.

ZIRLO (Zr-1.0Nb-1.0Sn-0.1Fe [9]) had outer diameter of 9.50 mm and a wall thickness of 0.57 mm. Prior testing, ZIRLO samples were hydrogen-charged by gaseous diffusion similar to processes in refs. [10,11]. The resultant hydride microstructure contained circumferential hydrides at hydrogen contents of 168 and 1554 wt. ppm.

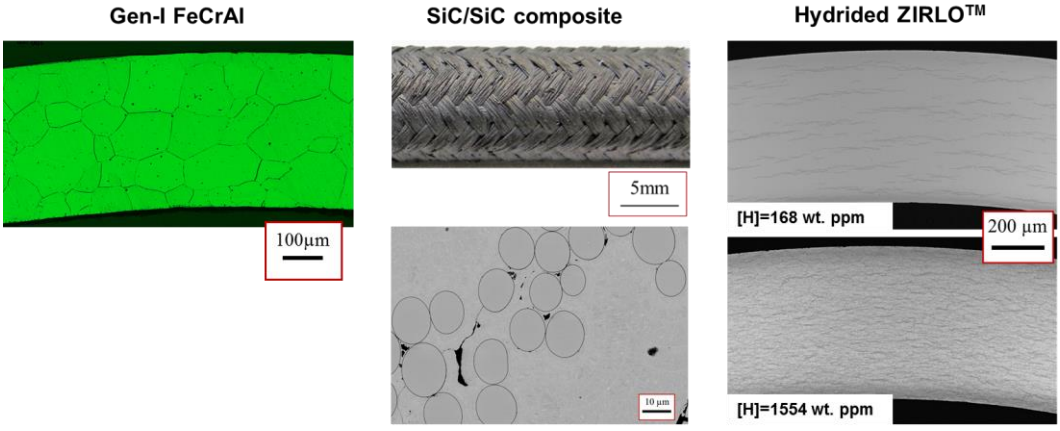

Fig. 1 Microstructure of the materials subjected to the modified-burst test

III. MECHANICAL PULSE CONTROLLED MODIFIED-BURST TEST

The working principle of the modified-burst test setup [7] is based on pressurizing a highly viscous hydraulic oil by the axial movement of a core pin, as depicted in Fig 2a (i) and (ii), at high speed (the maximum is 2.54 m/s) within an age-hardened Inconel 718 tube (driver tube) with a thickness of 0.98 mm and thinned-region thickness of 0.45 mm, as shown in Fig. 2a. Pressurization of the hydraulic oil induces expansion of the thinned region (pocket) of the driver tube [Fig. 2a (iii)]. This expansion is analogous to UO_2 pellet expansion during RIA; the expanding pocket strains the cladding tube placed around it. Thus, rupture or permanent deformation of the specimen occurs if the driver tube expansion induces sufficient strain at the contact area between the sample and the driver tube. The hydraulic oil pressure is recorded by a pressure transducer connected to driver tube and the hoop strain is measured by the strain gauge attached to the specimen surface. Extended-range Vishay Micro-Measurements strain gauges were attached to the specimen surface with Micro-Measurements M-Bond AE-15 to measure in situ hoop strains up to 10%[3] during loading. The strain gauges were connected to an analog data acquisition channel to improve the strain-reading rates at very high core-pin velocities. The mechanical tests reported in this study were performed at ambient temperature.

The rate and amplitude of the mechanical pulse is finely tuned by manipulation of the core-pin displacement and speed through the driver tube, as shown in Figs. 2b and 2c. The goals of mechanical pulse control are to elucidate any impact of the strain rate on the failure of the cladding and to be capable of simulating RIA scenarios over a range of pulse widths. The parameters that dictate the motion of the core-pin into the driver tube are the displacement and the speed of the core pin, both of which were controlled using a hydraulic press with precise displacement control.

Fig 2b shows that as displacement of the core-pin increase the internal pressure of the driver tube increases. Thus, the core-pin displacement affects the amplitude of the internal pressure, which corresponds to amount of energy deposited during a potent RIA event. Contrary to the magnitude of the core-pin displacement, Figure 2c depicts that increasing core-pin speed reduces the time to increase pressure, which corresponds to the duration of a RIA event. In conclusion, the ability to control of the core-pin displacement and speed enables to produce a variety of RIA scenarios for different ATF cladding candidates.

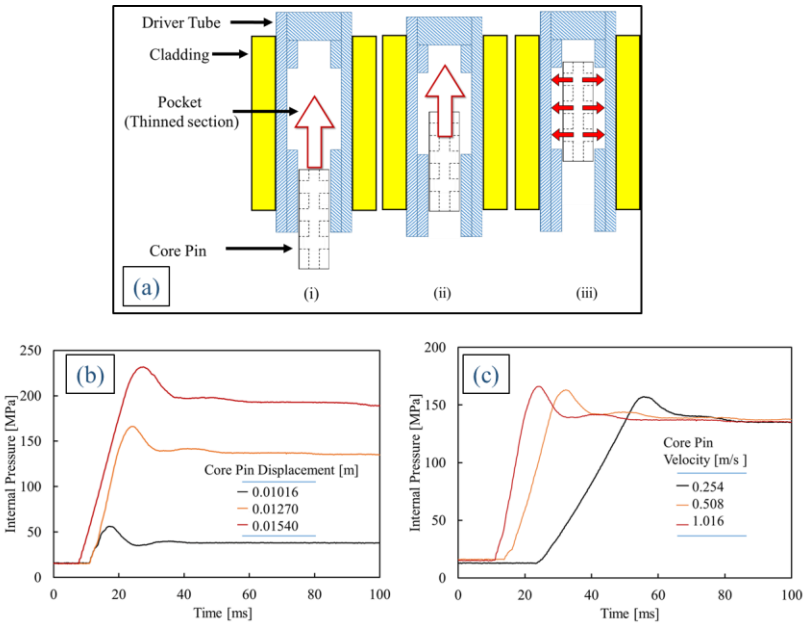

Fig. 2 (a) The axial cross section schematic of the modified-burst test. The effect of the parameters: displacement (b) and speed (c) of core-pin which control the mechanical loading.

[3] The maximum strain to be measured by the extended-range strain gauges limits the hoop strain measurement for ductile materials to 30% [24].

IV. RESULTS

The modified-burst test instrument developed for ATF cladding candidates was examined by conducting screening mechanical tests on unirradiated Gen-I FeCrAl, SiC/SiC and ZIRLO tube specimens. Similar mechanical pulses were applied to the specimens (internal pressure rise-time is about 10 ms and the final pressure values were not same because of dissimilar strength of different materials tested) and specimens were deformed to cause rupture. Also, internal pressures decreased to zero because the driver tubes failed due to rupture at the end of the test. Figs. 3a and 3b show the evolution of the internal pressure in the driver tube and hoop strain. The ZIRLO sample with low hydrogen content (168 wt. ppm) shows ductile failure at hoop strain of 9.2% whereas the ZIRLO sample with high hydrogen content (1554 wt. ppm) ruptures at hoop strain of 2.5%. The reduction in the failure strain with increasing hydrogen contents is due to the hydride-induce embrittlement in zirconium-based cladding alloys and is consisted with the previous studies [12,13]. The reason for the fluctuations in the hoop strain which were recorded at ~16 ms and ~20 ms by the strain-gauge for the sample with 168 wt. ppm of hydrogen is not fully understood. Some hypotheses for this behavior are: (i) these are experimental artifacts that were caused by the mechanical instrument's vibrations due to the core-pin impact and (ii) there were dislocation oscillations during plastic deformation due to the high strain rates of ~50 s^{-1}.

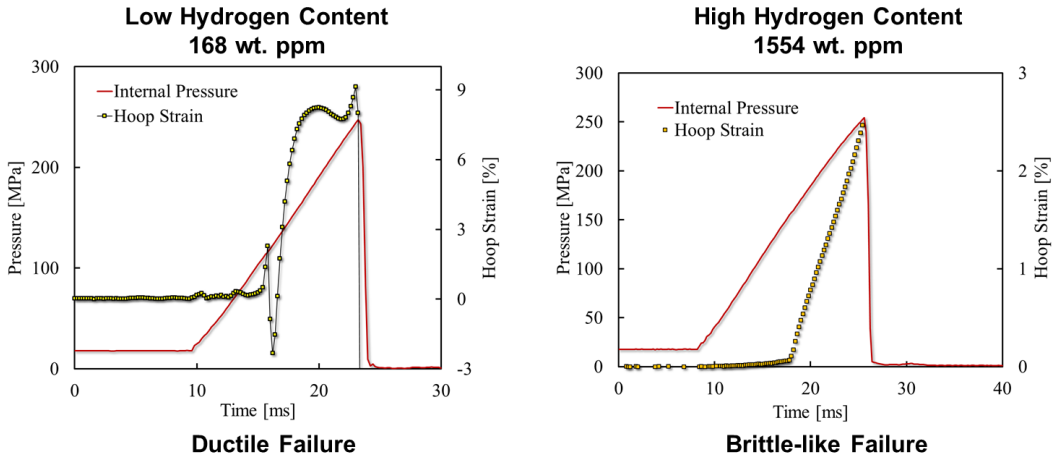

Fig. 3 Driver tube internal pressure and hoop strain responses of hydrided ZIRLO specimens with 198 wt. ppm of hydrogen (a) and 1554 wt. ppm of hydrogen (b)

Fig. 4 shows the example hoop strain evolution of FeCrAl specimen that is subjected to the same mechanical loading applied to ZIRLO™ sample. The FeCrAl sample did not rupture for the first attempt, but deformed plastically (the residual strain was determined as ~1%) as indicated in Fig. 4. Sample, then, was re-subjected to the same mechanical loading and failed at 5% of strain. Because of the prior damage, sample catastrophically failed[4]. The FeCrAl samples did not fail at the first trial of mechanical loading due to their extensive ductility although the yield strength of Gen-I FeCrAl is lower to other versions of this alloy family [8].

[4] The failure strain cannot accurately be determined from the second trial since the existing damage from the first trial is expected to have altered the materials properties of the sample. However, a lower limit for the failure strain can be speculated to be around 6% of hoop strain.

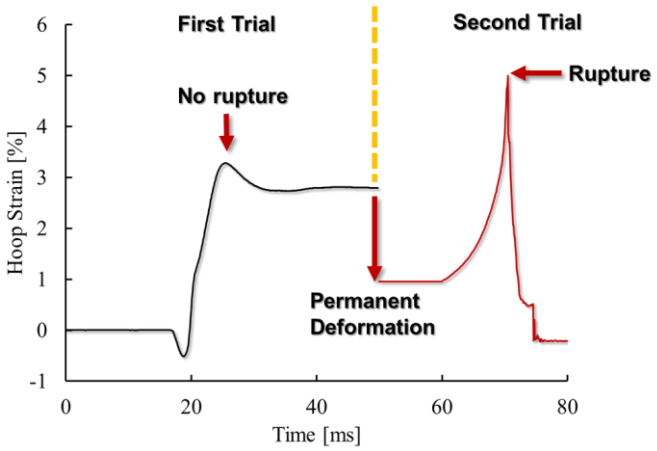

Fig. 4 Hoop strain evolution of Gen-I FeCrAl sample. Mechanical pulse imposed on the driver tube was same as that of applied to ZIRLO™ cladding

Fig. 5 shows the evolution of the internal pressure of the driver tube and the hoop strain on the sample surface. The triaxially-braided SiC/SiC composite sample fails at hoop strain of ~0.25%. The failure strain shown in Fig. 5 is higher than the brittle monolithic SiC [14] due to the reinforcement of the composite by three-dimensional architecture and the failure strain is consisted with the previous studies as reported by Katoh et al. [15]. A small decrease in hoop strain was recorded by the strain gauge between 10 to 20 ms. This is likely caused by the initial axial movement of the driver tube because of core-pin impact. The axial movement of the driver tube induces in-plane friction at the sample driver tube interface, which causes a small net axial tension until the sample's deformation is dominated by the hoop expansion of the driver tube. Therefore, the tension in the axial direction causes small amount of contraction in the hoop direction.

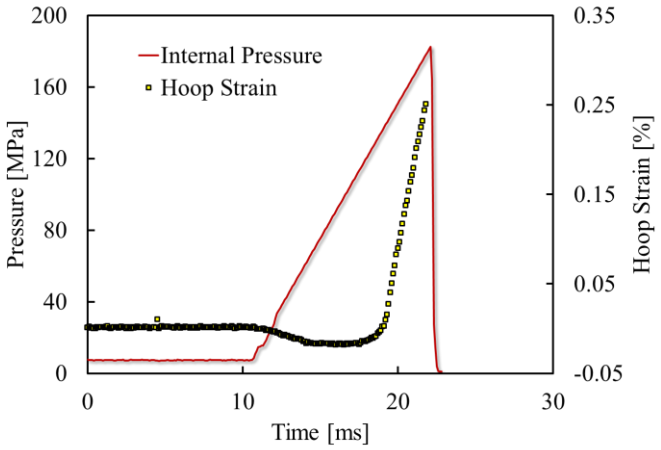

Fig. 5 Internal pressure of the driver tube and hoop strain evolution of SiC/SiC composite sample

The measured hoop strain of the tested samples at fracture [5] is expected to inform the model development for the ATF cladding candidates for nuclear reactor application. The prediction of the crack initiation and growth mechanisms is essential to develop PCMI-induced failure models during RIA. Fig. 6 shows the macroscopic fracture mode of the tested

[5] For a complete conclusion on the strain values and the cladding behavior subjected to the modified-burst test, more tests are being planned using digital image correlation set up.

samples at same conditions. Because high hydrogen contents used in this study to depict the effect of hydrogen on ZIRLO cladding is unrealistic for alloys in service, it was excluded.

Hydrided ZIRLO after modified-burst test (see Fig 6a) showed a hoop rupture associated with plastic deformation and following axial split, which was similar to the zirconium-based cladding alloys subjected to the integral tests [16,17]. Similar hoop rupture in ZIRLO was determined in Gen-I FeCrAl, but the axial split of the Gen-I FeCrAl was partially avoided by the multiple crack growth directions, as shown in Fig 6b.

SiC/SiC composite sample in Fig. 6c showed the hoop rupture behavior like other samples but without plastic deformation due to brittle nature of SiC. On the other hand, axial split was completely avoided in SiC/SiC composite sample because of strength reinforcement by the triaxially-braided fiber composite architecture.

During these example modified-burst tests, samples (including SiC/SiC) were subjected to the straining caused by the isotropic expansion of the driver tube until the initiation of the plastic instability. Up to this point, the sample is subjected to isotropic hoop expansion. The localization of the strain in the driver tube also induces a localized straining of samples. This type of deformation enables reproducing the macroscopic failure of samples that is similar to the expected PCMI loading during RIA.

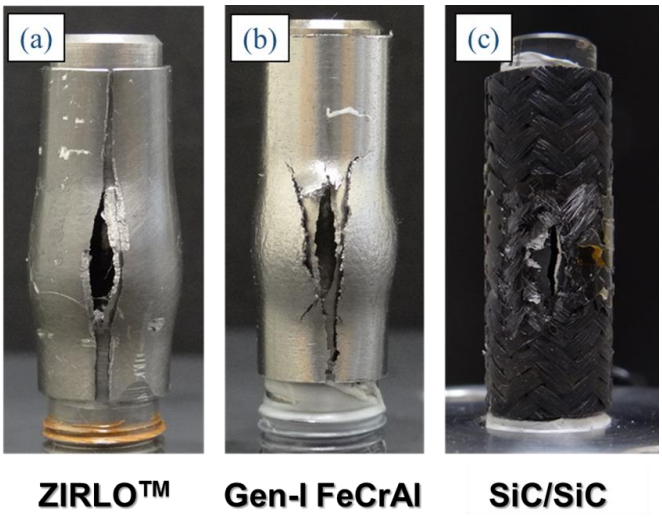

Fig. 6 Macroscopic failure modes of the specimens ZIRLO™ (168 wt. ppm of hydrogen) (a), Gen-I FeCrAl (b), and SiC/SiC (c) which were subject to modified-burst test at same mechanical loading conditions.

The details of the fracture surfaces of the samples are shown in Fig. 7. Hydrided ZIRLO (168 wt. ppm) consists of cracks of the circumferential hydride platelets and ductile α-zirconium matrix (see Fig. 7a). This microstructure indicates that the damage accumulated by void initiation at the hydride tips (or void initiation as a result of hydride cracking [13]), strain-induced void growth/linking developed until a small crack formed, and the specimen ruptured as a result of crack propagation through the sample thickness along the axial direction as shown in Fig. 6a [18].

The fracture surface of the Gen-I sample indicates cleavage fracture around a plastically deformed region, as shown in Fig. 7b. [18]. The mechanical damage was accumulated by ductile process of void initiation at grain boundaries or second phase particles (i.e. carbides) during the first load. However, initated cracks were arrested because the high fracture toughness of the material. For the second test, the cleavege patterns were observed due to the loss of toughness as caused by the prior damage in the first test.

Although the deformation of SiC/SiC samples is complicated due to the fiber architecture and the straining conditions (strain-driven deformation at transient loading conditions), the fracture surface of the SiC/SiC sample (see Fig 7c) indicates the rupture of pulled-out fibers and multi directional matrix cracking. This observation is consistent with literature data [19,20]. Thus, damage mechanism for SiC/SiC can be described by micromechanics approach to the brittle matrix composites [21] as follows: (i) the microcracks which are initally formed at macropores due to the stress concentration propagates through the SiC matrix, (ii) fiber microcracking and matrix debonding starts. Up to this stage, the mechancial load is shared by SiC fiber bundles and SiC matrix. As deformation continues the load sharing shifts to the SiC fiber

bundles, (iii) Once matrix cracking and debonding reaches to saturation, the load sharing ends and load is only carried by SiC fiber bundles, (iv) ultimate failure occurs when fibers loss their load-carrying capability at the maximum load.

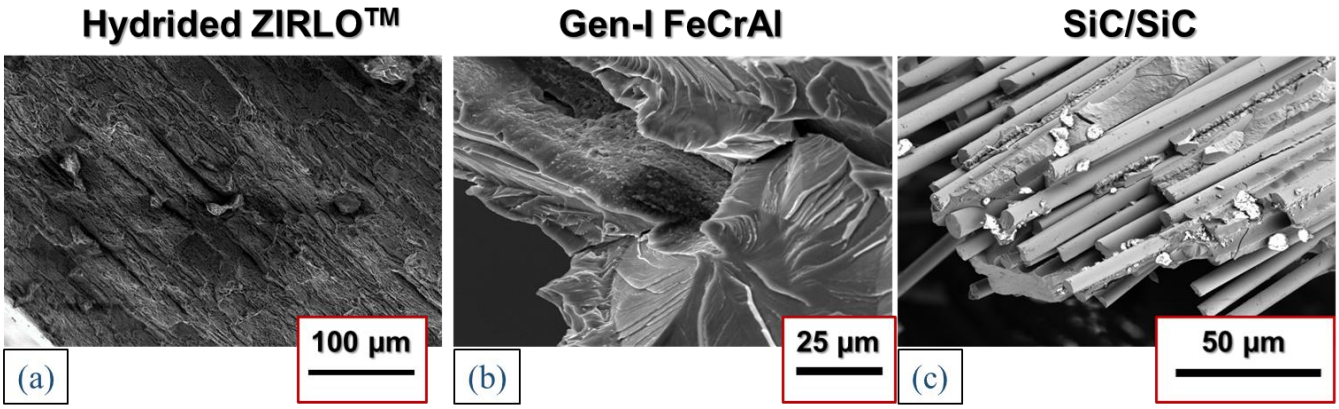

Fig. 7 Fracture surfaces of the tested specimens ZIRLO™ (a), Gen-I FeCrAl (b), and SiC/SiC (c).

V. CONCLUSIONS

A pulse- controlled modified-burst test was built for ATF cladding materials by simulating mechanical straining of the cladding by the thermal expansion of the fuel pellet during an RIA. Independent control of the mechanical pulse of the modified-burst test enabled to replicate different RIA scenarios for ATF cladding candidates.

Mechanical behavior of selected ATF cladding candidates (Gen-I FeCrAl and SiC/SiC) and a zirconium-based cladding (pre-hydrided ZIRLO) was tested under same mechanical loading conditions. ZIRLO (with 168 wt. ppm) and FeCrAl failed by ductile process, whereas ZIRLO (with 1554 wt. ppm) and SiC/SiC were ruptured at low hoop strains. Failure modes of all samples showed that the initial crack formation occurred in the hoop direction and axial crack propagation was occurred in ZIRLO (with 168 wt. ppm) and Gen-I FeCrAl. On the other hand, the three-dimensional composite architecture avoided the axial crack propagation in SiC/SiC composite sample.

ACKNOWLEDGMENTS

This work was supported by the US Department of Energy Office of Nuclear Energy Advanced Fuels Campaign. The aid and technical assistance of Ken Yueh at Electric Power Research Institute was critical and is gratefully acknowledged. Useful discussion with Dan Wachs at Idaho National Laboratory is also acknowledged. Authors are thankful of Rick Lowden and Donald III Erdman during mechanical test device construction. Also, we are thankful to Aida Amroussia for SEM pictures, and Tom Geer and Sun Zhiqian for optical micrographs.

REFERENCES

[1] K.A. TERRANI, S.J. ZINKLE, L.L. SNEAD, Advanced oxidation-resistant iron-based alloys for LWR fuel cladding, J. Nucl. Mater. 448 (2014) 420–435. doi:10.1016/j.jnucmat.2013.06.041.

[2] L. HALLSTADIUS, S. JOHNSON, E. LAHODA, Cladding for high performance fuel, Prog. Nucl. Energy. 57 (2012) 71–76. doi:10.1016/j.pnucene.2011.10.008.

[3] S.J. ZINKLE, K.A. TERRANI, J.C. GEHIN, L.J. OTT, L.L. SNEAD, Accident tolerant fuels for LWRs: A perspective, J. Nucl. Mater. 448 (2014) 374–379. doi:10.1016/j.jnucmat.2013.12.005.

[4] N.R. BROWN, M. TODOSOW, A. CUADRA, Screening of advanced cladding materials and UN–U3Si5 fuel, J. Nucl. Mater. 462 (2015) 26–42. doi:10.1016/j.jnucmat.2015.03.016.

[5] C.P. MASSEY, K.A. TERRANI, S.N. DRYEPONDT, B.A. PINT, Cladding burst behavior of Fe-based alloys under

LOCA, J. Nucl. Mater. 470 (2016) 128–138. doi:10.1016/j.jnucmat.2015.12.018.
[6] U.S. NRC, NRC: 10 CFR Appendix A to Part 50—General Design Criteria for Nuclear Power Plants, n.d. https://www.nrc.gov/reading-rm/doc-collections/cfr/part050/part050-appa.html.
[7] K. YUEH, J. KARLSSON, J. STJÄRNSÄTER, D. SCHRIRE, G. LEDERGERBER, C. MUNOZ-REJA, L. HALLSTADIUS, Fuel cladding behavior under rapid loading conditions, J. Nucl. Mater. 469 (2016) 177–186. doi:10.1016/j.jnucmat.2015.11.032.
[8] Y. YAMAMOTO, B.A. PINT, K.A. TERRANI, K.G. FIELD, Y. YANG, L.L. SNEAD, Development and property evaluation of nuclear grade wrought FeCrAl fuel cladding for light water reactors, J. Nucl. Mater. 467 (2015) 703–716. doi:10.1016/j.jnucmat.2015.10.019.
[9] G.P. SABOL, G.R. KILP, M.G. BALFOUR, E. ROBERTS, Development of a Cladding Alloy for High Burnup, in: L.F.P.V. Swam, C.M.Eucken (Eds.), Eighth Int. Symp. Zircon. Nucl. Ind., ASTM, San Diego, 1989: pp. 227–244.
[10] X. HU, K.A. TERRANI, B.D. WIRTH, Hydrogen desorption kinetics from zirconium hydride and zirconium metal in vacuum, J. Nucl. Mater. 448 (2014) 87–95. doi:10.1016/j.jnucmat.2014.01.028.
[11] M.N. CINBIZ, D.A. KOSS, A.T. MOTTA, The influence of stress state on the reorientation of hydrides in a zirconium alloy, J. Nucl. Mater. 477 (2016) 157–164. doi:10.1016/j.jnucmat.2016.05.013.
[12] M.A. MARTIN-RENGEL, F.J. GÓMEZ SÁNCHEZ, J. RUIZ-HERVÍAS, L. CABALLERO, Determination of the hoop fracture properties of unirradiated hydrogen-charged nuclear fuel cladding from ring compression tests, J. Nucl. Mater. 436 (2013) 123–129. doi:10.1016/j.jnucmat.2013.01.311.
[13] M. LE SAUX, J. BESSON, S. CARASSOU, C. POUSSARD, X. AVERTY, Behavior and failure of uniformly hydrided Zircaloy-4 fuel claddings between 25 °C and 480 °C under various stress states, including RIA loading conditions, Eng. Fail. Anal. 17 (2010) 683–700. doi:10.1016/j.engfailanal.2009.07.001.
[14] L.L. SNEAD, T. NOZAWA, Y. KATOH, T.-S. BYUN, S. KONDO, D.A. PETTI, Handbook of SiC properties for fuel performance modeling, J. Nucl. Mater. 371 (2007) 329–377. doi:http://dx.doi.org/10.1016/j.jnucmat.2007.05.016.
[15] Y. KATOH, K. OZAWA, C. SHIH, T. NOZAWA, R.J. SHINAVSKI, A. HASEGAWA, L.L. SNEAD, Continuous SiC fiber, CVI SiC matrix composites for nuclear applications: Properties and irradiation effects, J. Nucl. Mater. 448 (2014) 448–476. doi:10.1016/j.jnucmat.2013.06.040.
[16] F. NAGASE, T. FUKETA, Investigation of hydride rim effect on failure of Zircaloy-4 cladding with tube burst test, J. Nucl. Sci. Technol. 42 (2005) 58–65. doi:10.1080/18811248.2005.9726364.
[17] T. SUGIYAMA, M. UMEDA, T. FUKETA, H. SASAJIMA, Y. UDAGAWA, F. NAGASE, Failure of high burnup fuels under reactivity-initiated accident conditions, Ann. Nucl. Energy. 36 (2009) 380–385. doi:10.1016/j.anucene.2008.12.003.
[18] J.H. KIM, M.H. LEE, Y.H. JEONG, J.G. LIM, Behavior of zirconium fuel cladding under fast pressurization rates, Nucl. Eng. Des. 238 (2008) 1441–1447. doi:10.1016/j.nucengdes.2007.10.020.
[19] C. DROILLARD, J. LAMON, Fracture Toughness of 2-D Woven SiC/SiC CVI-Composites with Multilayered Interphases, J. Am. Ceram. Soc. 79 (1996) 849–858. doi:10.1111/j.1151-2916.1996.tb08516.x.
[20] N. CARRÈRE, E. MARTIN, J. LAMON, The influence of the interphase and associated interfaces on the deflection of matrix cracks in ceramic matrix composites, Compos. Part A Appl. Sci. Manuf. 31 (2000) 1179–1190. doi:10.1016/S1359-835X(00)00095-6.
[21] J. LAMON, A micromechanics-based approach to the mechanical behavior of brittle-matrix composites, Compos. Sci. Technol. 61 (2001) 2259–2272. doi:10.1016/S0266-3538(01)00120-8.
[22] M. NEDIM CINBIZ, N. BROWN, K.A. TERRANI, R.R. LOWDEN, D. ERDMAN, The Mechanical Response Evaluation of Advanced Claddings During Proposed Reactivity Initiated Accident Conditions, in: X. Liu, Z. Liu, K. Brinkman, S. Das, S. Dryepondt, J.W. Fergus, Z. Guo, M. Han, J.A. Hawk, T. Horita, P. Hosemann, J. Li, E. Olivetti, A. Pandey, R.B. Rebak, I. Roy, C. Shang, J. Zhang (Eds.), Energy Mater. 2017, Springer International Publishing, Cham, 2017: pp. 355–365. doi:10.1007/978-3-319-52333-0_32.
[23] M.N. CINBIZ, N.R. BROWN, K.A. TERRANI, R.R. LOWDEN, D. ERDMAN, A pulse-controlled modified-burst test instrument for accident-tolerant fuel cladding, Ann. Nucl. Energy. 109 (2017) 396–404. doi:10.1016/j.anucene.2017.05.058.
[24] K.-F. NILSSON, M. NÉGYESI, Z. SZÁRAZ, I. SIMONOVSKI, An evaluation of the segmented expanding cone-mandrel test to assess hydride re-orientation and ductility reduction for Zircaloy-2 cladding tubes, J. Nucl. Mater. 466 (2015) 220–233. doi:10.1016/j.jnucmat.2015.07.019.